NASA TN D-1889

34 p.

TECHNICAL NOTE
D- 1889

THE INFLUENCE OF HEATING RATE AND TEST STREAM OXYGEN CONTENT ON THE INSULATION EFFICIENCY OF CHARRING MATERIALS

By Nick S. Vojvodich and Ernest L. Winkler

Ames Research Center
Moffett Field, Calif.

NATIONAL AERONAUTICS AND SPACE ADMINISTRATION
WASHINGTON
July 1963

NATIONAL AERONAUTICS AND SPACE ADMINISTRATION

TECHNICAL NOTE D-1889

THE INFLUENCE OF HEATING RATE AND TEST STREAM OXYGEN CONTENT ON THE INSULATION EFFICIENCY OF CHARRING MATERIALS

By Nick S. Vojvodich and Ernest L. Winkler

SUMMARY

The insulation behavior of thin sections (1/10 of an inch) of some typical charring materials was studied at cold-wall convective heating rates between 5 and 120 Btu/ft^{2}sec in both arc-heated nitrogen and air. The insulation efficiency (the total cold-wall heat input per initial pound of material for a backface temperature rise of 300° R) was used as a figure of merit in this investigation.

Test results indicate that in both nitrogen and air the insulation efficiency is reduced as the heating rate is reduced. Furthermore, at the same cold-wall heating rate, the insulation efficiency measured in air was always lower than in nitrogen with the most pronounced reduction occurring at the lowest heating rates. Temperature measurements of the material surfaces were higher in air than in nitrogen, suggesting that the effect of air environment on material performance is a consequence of exothermic combustion reactions.

INTRODUCTION

In choosing a thermal protection system for a reentry vehicle, the effect of both the magnitude and the duration of the heat pulse must be considered. For example, an ablation system which is highly effective in protecting the stagnation area of a ballistic vehicle may not be suitable for protecting the afterbody of a lunar return vehicle. The heating of such an afterbody is at a relatively low rate but of long duration, making the over-all thermal diffusivity of the system of prime importance. The majority of experimental investigations to date have considered the mass loss performance of materials at high heating rates. The rate at which heat is conducted into ablative materials has been studied (refs. 1 to 4), but the studies were made at heating rates greater than 50 Btu/ft^{2}sec which are characteristic of those encountered by the front face of entry bodies.

Since insulation data are needed for the high-energy, long-time, low-heating rate environment expected on afterbodies, the present investigation was initiated to determine the influence of low heating rates on the insulation effectiveness of thin sections of some typical composite ablative materials. The materials were tested in a high-energy, arc-heated stream at high as well as low heating rates so that the data might be compared directly to the results of reference 1. The present tests were conducted in both air and nitrogen to determine the effect of gas composition on the behavior of these materials. The results of these experiments are reported herein.

NOTATION

a_1, a_2, a_3	constants defined by equations (3) and (4)
E	test stream energy
E_t	total input energy, $\frac{0.948\ P}{\dot{w}}$, Btu/lb
L	test sample thickness, ft
P	power supplied to electrodes, kw
Q	total cold-wall heat input, $q(t_{\Delta T=300})$, Btu/ft^2
q	cold-wall convective heating rate, Btu/ft^{2}sec
q_r	radiative heating rate, Btu/ft^{2}sec
t	time, sec
T	temperature, $^\circ$R
T_{br}	brightness temperature, $^\circ$R
w	test gas flow rate, lb/sec
W	initial weight per unit area, $\rho_i L_i$, lb/ft^2
x	distance normal to surface
ΔT	temperature rise at back surface, $(T - T_i)_{x=L}$, $^\circ$R
ϵ	surface emissivity
λ	wavelength, ft
ρ	density, lb/ft^3

Subscripts

a	afterbody
i	initial
s	stagnation point

EXPERIMENT

Facility

The materials were tested in a 4-inch-diameter, high-energy, supersonic, dissociated-gas stream generated by the fully water-cooled arc-jet wind tunnel, described in detail in references 5, 6, 7. The nominal conditions of the free jet test stream were: Mach number, 5.5; static pressure, 2.5×10^{-4} atm; impact pressure, 0.01 atm; and test gas flow rate, 0.005 lb/sec. The total input energy level to the arc was varied from 5,000 to 13,000 Btu/lb by changing the electrical input energy. The variation of test stream energy with total input energy (as determined by the technique outlined in ref. 5) is shown in figure 1 and demonstrates little change in performance when air was used in place of nitrogen as the test gas. These stream conditions provided two ranges of convective heating rates, from 5 to 10 and from 40 to 120 Btu/ft^{2}sec, depending on the model configuration.

Models

Insulation models.- Since the stream energy was the only test condition varied, two different model configurations were necessary to obtain the required range in heating rates. By locating the test samples on the afterbody of a hemisphere-cylinder, where the static pressure was low, it was possible to obtain the low convective heating rates of primary interest in this investigation and still test at high stream energies. Conversely, data for high heating rates were obtained at the stagnation point where the pressure was high. Two different configurations of afterbody samples constructed of the test materials were used. Model 1 had a half-cylinder sample as shown in figure 2(a), and model 2 had a full cylinder sample as shown in figure 2(b). In contrast to model 1, the sample of model 2 had no circumferential or longitudinal air gaps isolating it from the body. Hence, model 2 was used to assess the effect of these gaps on the flow over the test sample of model 1. As noted in figure 2(b), model 3 had the same test sample geometry as model 2, but the cooled hemispherical section was replaced with one machined of the test material so that the effects of upstream mass injection on the behavior of the material could also be measured. High heating rates were obtained by placing the test sample at the stagnation point of a flat-faced cylinder (see fig. 2(c)). Both configurations placed the test samples in a region of relatively uniform heating rate. Test samples were constructed of the following materials:

Materials						Models			
N, percent	P, percent	PM, percent	Q, percent	M, percent	ρ, lb/ft^3	1	2	3	4
50	50				75	X			X
50	25	25			45	X	X	X	X
					36	X			X
50	22.5	22.5	5		35	X			X
	11.2	33.8	5	50	62	X			X
Cork composition					29	X			X

N	nylon	Q	quartz fibers
P	phenolic resin	M	Melamine
PM	phenolic microballoons	percent	weight fraction

Heating rate models.- The cold-wall convective heat-transfer rates at the respective test locations were determined with transient type calorimeter models. For the afterbody rates, half and full cylinder copper calorimeters, which had external dimensions identical to the test samples, were supported in models 1 and 2 with small contact area to minimize conduction heat losses (see fig. 3(a)). The calorimeter model shown in figure 3(b) was used to measure the stagnation-point heating rates.

Test Procedure and Measurements

Before the material samples were tested, stream properties and cold-wall heating rates were measured at a number of arc input energy levels so that the desired environmental test conditions could be selected. The technique for testing the materials was similar to that outlined in reference 5. Briefly, the test samples were placed in the model body, which was located on the stream center line with the stagnation point 1 inch downstream of the nozzle exit plane. The resistance of each thermocouple was measured, the test sample was carefully alined, and the test chamber was evacuated. To eliminate the effects of stream starting transients, a split tubular shield was placed over the model covering the test sample area. The arc was initiated and the nozzle wall and box pressure were balanced. To achieve balanced flow, the exit pressure of the nozzle was matched with the test stream static pressure by throttling the vacuum system. When steady flow conditions existed, the shield was quickly removed, thereby exposing the model to a step heat pulse. Front and back surface temperatures of the sample were monitored and when the temperature rise of the back surface exceeded 300° R, the tests were terminated. During the test each sample was photographed with a 16-mm motion picture camera to obtain a time record of surface phenomena.

Heating rates.- The calorimeter technique of measuring cold-wall convective heating rates in high-energy streams has been described in detail in both references 5 and 8. The method requires the measurement of the temperature-time

history of a thermally insulated calorimeter having mass, m, surface area, A, and specific heat, c_p. The initial slope of this curve, $(dT/dt)_i$, and the material properties are combined in the equation:

$$q = \frac{mc_p}{A}\left(\frac{dT}{dt}\right)_i$$

to yield the heating rate in the absence of ablation. The variation of both afterbody and stagnation-point heating rates with total energy input for nitrogen is given in figure 4. The solid lines represent the least squares fit calculated from the data. The dashed line is the theoretical variation of the heating rate, q_a, to the cylindrical afterbody with stream energy, and was calculated by combining the heat-transfer ratio, q_a/q_s, given in reference 9, with the stagnation-point rate, q_s, obtained by modifying the flat-faced cylinder data to take account of the difference in stagnation point velocity gradient. The agreement between the theory and least squares fit line is well within the deviation of the data from the solid line. It was assumed in the calculation of reference 9 that the flow over the afterbody was both laminar and attached. The agreement of the afterbody heat-transfer data with the theory thus suggests that the flow over the afterbody heat-transfer model was also attached and laminar. It is not possible to make the same assumption regarding the flow over the test sample, since the radial dimension of the sample was reduced during the test. The question then arises as to the possibility of separation occurring in this cavity formed by ablation and the effect of the separated flow on the average heat-transfer rate to the sample. Therefore, to investigate the effect of dimension change on heating rate, heat-transfer measurements were repeated with the calorimeter shown in figure 3(a), having the upper surface stepped 0.050 inch below the contour of the body. The data obtained with this model are presented in figure 4 and are in substantial agreement with the smooth contour data, indicating that the flow, if separated, reattaches very close to the origin of the step. These data exhibit the same trend as the data and theory of Larson for very highly cooled walls (ref. 10).

The high and low heating-rate measurements were repeated in air to see whether the test gas composition had any effect on the cold-wall heating rate levels. It is noted in figure 4 that the measurements obtained in air agreed over the entire stream energy range with the heating rates obtained previously in nitrogen.

Back-face temperature measurements.- The back-face temperature history of all the test samples was determined using chromel-alumel thermocouples attached to a thin copper substrate cemented to the rear face of the samples with RTV 60 resin bond: A small percentage of 0.003-inch-diameter microbrite beads was added to duplicate the bond thickness used by Brooks, et al., in reference 1. The thermocouple junctions were peened into small holes drilled in the substrate to assure a good thermal contact. Chromel-alumel thermocouple wires of 0.005-inch diameter were used to minimize possible conduction losses. The over-all sensitivity of each thermocouple was obtained prior to testing the ablation models by measuring the thermocouple resistance R_{tc}. This resistance, the sensitivity of the thermocouple S_{tc} (millivolts per degree Rankine), and the

previously measured galvanometer resistance R_g and sensitivity S_g when substituted into the relationship

$$S = \frac{S_g\,(R_{tc} + R_g)}{S_{tc}},\ {}^{\circ}R/in.$$

yields the over-all sensitivity. The sensitivity calculated from this equation was checked for some of the thermocouples by immersing the substrate into two water baths at different temperatures, and the temperature difference divided by the difference in galvanometer deflections agreed very well with the calculated values.

Surface temperature measurements.- For the low heating rate tests conducted in nitrogen with the afterbody model, the surface temperatures were measured with a radiometer temperature transducer, which was mounted on the inside of the tunnel to avoid intervening optics. An image of the surface was focused on the radiometer thermocouples, and the output was read on a recorder.

The surface temperatures of the stagnation-point models exceeded the range of the radiometer transducer; hence, an optical pyrometer was mounted outside the tunnel so that the temperatures could be observed visually.

The radiometer was calibrated over the temperature range 540° to 2460° R by relating its output signal to the temperature of an oxidized, cast iron slug placed at the bottom of a deep, electrically heated, graphite crucible. The slope of this calibration curve, when compared to the slope of the black-body curve ($\epsilon = 1$) yielded an effective emissivity of 0.88 for the calibration system. Reference 11 reports that the emissivity of a typical phenolic nylon is also 0.88 in the temperature range 150° to 1100° R. No emissivity data existed for the phenolic material in its high-temperature charred conditions but for a comparable surface (rough carbon) the emissivity is 0.6 at 1900° R (see ref. 12). The difference between the emissivity of the test surface and calibration system requires that the following correction be applied to obtain the true surface temperature:

$$\frac{(T_{x=o})_{\epsilon}}{(T_{x=o})_{\epsilon=0.88}} = \sqrt[4]{\frac{0.88}{\epsilon}}$$

This expression, which was deduced from the radiaton equation $q_r = \epsilon\sigma(T_{x=o})^4$, yields a difference of only 9 percent when the emissivity of the surface is assumed to be 0.6. Since the emissivity is not known accurately, the uncorrected radiometer readings have been reported herein.

The optical pyrometer used to measure higher surface temperatures had been calibrated against a standard tungsten lamp which had in turn been calibrated by the National Bureau of Standards. The major source of error in measurements made with this instrument was the departure of the emissivity of the test surface from unity. The equation of reference 13 (given here in the nomenclature of the present report) may be used to calculate the true temperature from the

measured brightness temperatures.

$$\ln \epsilon(\lambda,T) = \frac{0.0849 \text{ ft } {}^{\circ}R}{\lambda} \left(\frac{1}{T} - \frac{1}{T_{br}}\right)_{x=0}$$

The equation yields a difference of 6 percent between the true temperature and the measured brightness temperature, provided the surface of the sample acts as a grey body (ϵ = 0.6 over entire spectral range). Once again, because the high-temperature emissivity is not known accurately, the brightness temperature has been reported as the surface temperature. Since the primary objective of this research program was to measure the back-face temperature rises, and because only the trends of the surface temperature with heating rate and stream composition were desired, the uncertainty in the measurements introduced by the radiometer and optical pyrometer were not considered serious.

RESULTS AND DISCUSSION

Experimental Data

Back-face temperature.- Typical variations of the back-face temperature with time for both stagnation-point (high heating rate) and afterbody (low heating rate) models (nos. 4 and 1, respectively) tested in air and nitrogen are presented in figure 5. The heating rate level and test gas composition both affect the shape of these curves. First, we note that at any time as the heating rate is increased, the temperature is also increased. Secondly, the gas composition has very little effect at the high heating rates, but results in a large difference in temperature at the lower heating rates. Finally, a comparison of the initial transients indicates that the heat pulse penetrates to the back face more rapidly at the higher heating rates.

Surface temperature.- The variations of surface temperature with time at heating rates comparable to those of figure 5 are shown in figure 6 for nitrogen and air. The behavior of the surface temperatures is analogous to that exhibited by the back-face temperature shown in figure 5; that is, higher surface temperatures occur at the higher heating rates and the gas composition has a more pronounced effect at the lower heating rates. The difference in the back-face temperature rise history at the lower heating rates (fig. 5) appears to be a direct consequence of the higher surface temperatures measured in air as shown in figure 6.

The variation of steady-state surface temperature with heating rate shown in figure 7 was obtained by the extrapolation of curves such as those shown in figure 6. Included in the figure are some unpublished temperature measurements obtained at Langley and Ames in high-energy test facilities at heating rates in excess of 200 Btu/ft^{2}sec. This plot indicates that the difference in surface temperature for samples tested in air and in nitrogen is most severe at low heating rates (4 to 13 Btu/ft^{2}sec) where the ratio of air to nitrogen surface temperature $(T_{air}/T_{N_2})_{x=0}$, is 1.68, while at higher heating rates this ratio

is only 1.06. We note also that at the low heating rate the surface temperatures determined in air with the radiometer and optical pyrometer are in good agreement. Furthermore, extrapolation of the stagnation-point surface temperature data obtained in air agrees with the trend of the unpublished measurements from Langley and Ames.

Insulation Time

The insulation time (time for the back face of the material to experience a temperature rise of 300° R) when combined with the cold-wall heating rate and initial weight per unit area yields the insulation efficiency, $\frac{Q}{W} = \frac{q(t_{\Delta T=300})}{W}$, which was previously defined in reference 1. The reasons for selecting this parameter for the evaluation of materials for the protection of low heating rate areas have been thoroughly discussed in references 1 and 2. However, a brief discussion of the 300° R back-face temperature rise limit is in order at this time. A heat shield may be attached to its substructure by a bonding agent, by mechanical means (e.g., bolts), or by a combination of the two. Mechanical methods usually employ fastening members which are attached to holes in the ablation material. Since there is some question as to the structural integrity of an ablation material which has a number of large holes, epoxy resin bonds have been proposed for joining the ablation material to the substructure. However, the strength of the majority of bonding agents decreases rapidly as the temperature is increased and reference 14 cites an upper safe limit of operation of about 1260° R. Thus, for an initial heat shield temperature of 540° R, if the back-face surface is limited to a 300° R rise, a 400° R factor of safety will exist for the design.

The effect of heating rate.- The variation of the ratio of insulation time to initial weight per unit area $\left(\frac{t_{\Delta t=300}}{W}\right)$ with heating rate for a 50-25-25 composite plastic is plotted in figure 8. The data were obtained with the combination of models, densities, and test gases shown in the following table:

Model	Figure	Density, lb/ft^3	Test gas	Facility
1	2(a)	36 45	N_2, air N_2, air	Present
2	2(b)	45	N_2	
3	2(b)	45	N_2	
4	2(c)	36 45	Air N_2, air	
		45	Air	Ref. 8

The afterbody data of model 1, when compared to the stagnation-point data of model 4, show that the insulation time is increased by a factor of 3 (in nitrogen) as the heating rate is decreased from 100 to 8 Btu/ft^{2}sec. Also contained in figure 8 are data from models 1 and 4 tested in air. It is seen immediately that the insulation performance of the test samples in this environment was lower than previouly obtained in nitrogen. The most severe reduction occurred at the lower heating rates. The effect of gas composition on the insulation efficiency will be discussed.

The solid line shown is the least squares correlation of the data obtained with the 45 lb/ft^3 material tested in nitrogen. The two broken lines are theoretical estimates of the variation of insulation time with heating rate. The upper line was calculated assuming that the material behaved in such a manner that time could be exchanged for heating rate, that is, for a given thickness of material $t_{\Delta T=300}$ = constant/q. It will be noted that if this method is used to predict insulation times for the low heating rates from high heating rate data, a considerable error will exist (a factor of 10). Munson and Spindler in reference 15 have derived a set of equations which describe the transient behavior of a composite material exposed to convective heating. The digital program for the solution of these equations was used on a 7090 IBM computer to obtain the temperature profile through the material at various times for a 0.1 inch thick sample of material exposed to heating rates and enthalpies corresponding to the test conditions. The calculated temperature rises were in reasonable agreement with the experimental data even though there was uncertainty in the intrinsic material properties, such as heat of degradation, and in the char layer properties. The calculations were adjusted to agree with the data at q = 60 Btu/ft^{2}sec, and the resulting trend is shown by the lower broken line. Thus, it is seen, both experimentally and analytically, that the insulation time is not inversely proportional to the heating rate as predicted by the simplified theory.

The effect of gas composition.- Two experimental observations indicated an additional heat flux to the surface of the test samples which were exposed to an oxidizing stream: First, the surface temperatures at both low and high heating rates were greater in air than in nitrogen (see fig. 7); second, a post-run inspection of the afterbody surfaces revealed that a considerable fraction of the active material (nylon) had melted and solidified on the samples tested in nitrogen. In air, however, the active material had completely vaporized. The results of reference 5 indicate that a higher heating rate is necessary for vaporization than for melting. This difference in heat flux can, perhaps, be accounted for by the combustion of vaporized species (homogeneous reactions) or by surface oxidation (heterogeneous reactions).

Therefore, additional back-face temperature-time responses of 0.1 inch thick samples of the test materials were obtained in the same facility with air as the test gas, at heating rates and enthalpies close to those for the nitrogen tests. The data from these tests are plotted in figure 8. The stream was contaminated, however, by tungsten from the arc heater electrodes, and to determine the effect of this contamination, the same material was tested at comparable stream conditions in the Ames concentric ring arc heater (described in ref. 8), which had a low contamination level. The data, also shown in figure 8, show that stream contamination did not alter the high heating rate data. Furthermore, the data obtained in air and nitrogen exhibit the same trend as the surface temperature

measurements; that is, for q greater than 20 Btu/ft^{2}sec, the insulation times agree closely, while at $q = 7$ Btu/ft^{2}sec, the insulation time measured in air is 1/3 lower than the least squares line fitted to the nitrogen data.

The combustion heating of ablating surfaces has been considered in detail for both homogeneous (gas phase) and heterogeneous (surface oxidation) reactions (see refs. 16, 17, 18). The scope of the present investigation did not include a determination of the type of reaction (gas or surface) or a detailed study of the resultant surface ablation. However, post-run inspections of the low heating rate models and measurements of the total mass lost by the samples did show that more material was lost in the air tests. These preliminary data indicate that the reactions are mainly heterogeneous, but further experimental study of this separate problem is necessary.

The effect of other parameters.- As previously stated, the primary purpose of the present study was to determine the influence of heating rate and test gas composition on the insulation behavior of a typical material. However, the effects of other test variables, namely, enthalpy, test sample geometry, upstream mass injection, material density, and material composition, on the test results were also considered. The influence of each of these variables will be discussed in the order given.

Enthalpy: References 5 and 8 are representative of the many experimental studies of materials which depolymerize to a gas at a relatively low temperature. These tests have indicated that the primary heat blockage mechanisms of such materials is the surface shielding due to mass injection, a process which is highly dependent on stream enthalpy. It is logical then, to question the experimental technique of the present study in which the effect of heating rate, at a given body location, on the material behavior was obtained by changing the enthalpy. In contrast to the relatively simple blowing phenomena occurring at the surface of a subliming material, the decomposition of a charring material is a highly complex internal process, which has been described thoroughly in the literature (see, e.g., ref. 1). As indicated by the data of reference 4, the primary rejection of heat is accomplished by reradiation from the high surface temperatures so that one would not expect enthalpy to have a strong effect on the internal behavior of a charring material. This supposition is substantiated to a degree, by the data of figure 8(a) where the variation of insulation time with heating rate appears to be independent of the enthalpy which has been changed by a factor of 2 in both the low and high heating rate tests. This observation is certainly not adequate verification; therefore, let us consider some additional experimental measurements performed at the same heating condition, but obtained by two different modes of heating. The most pertinent information is contained in reference 1 which discussed test results obtained with samples heated convectively at 100 Btu/ft^{2}sec in a 3000 Btu/lb stream and radiantly in the absence of any high enthalpy flow. It is shown that the time for the back face to experience a 300° R rise was the same in both cases. Furthermore, the data were repeated at a number of heating rates and it was concluded that the mode of heating did not alter the performance of the charring composite plastic tested. It is of interest to note that the data point in figure 8(a) at 20 Btu/ft^{2}sec was obtained in a vacuum with a radiant source and yet agrees with convective heating data. R. Dickey and J. Haacker, who obtained that point, also made measurements

at high convective heating rates in air at enthalpies much lower than those of the present investigation; yet, as shown in figure 8(a), the two sets of data agree. When all of this information is considered, it appears that enthalpy plays only a secondary role in influencing the behavior of high-temperature charring composite materials.

Test sample geometry: The results of the tests of model 2, which had a full cylinder test sample, are plotted in figure 8(a). Comparison of these data with those previously obtained with model 1 indicated that the air gap, which separated the half cylinder test sample from the body of model 1, had little effect on the performance of the material; that is, no appreciable internal flow occurred nor was the heat transfer to the sample altered by the presence of the insulation gap.

Mass injection: The nose segments of both models 1 and 2 were water cooled. This raised the question of what effect upstream mass injection would have upon the heating rate and subsequent behavior of the afterbody test samples. To investigate this question in detail, model 2 was modified by replacing the water-cooled section ahead of the test sample with segments similar in geometry but machined of the test material (see fig. 2). This configuration (model 3) was tested in nitrogen and motion pictures were taken of each run. In contrast to models 1 and 2, where the origin of the ablation layer coincided with the leading edge of the test sample, these pictures revealed that the nose section immediately began to ablate and the resultant highly luminous layer of injected gases covered the entire model. In spite of this apparent large increase in mass injection ahead of the test sample, the data from model 3 agreed with that previously obtained with models 1 and 2 (see fig. 8(a)). It appears, then, that the local mass injection occurring at the test sample is more important in determining the local rate of heat transfer than the mass injection occurring upstream of the sample.

Material density: The effect of initial material density on insulation time was measured at both low and high heating rates. The data, included in figure 8(a), indicate that the insulation times measured with the low-density samples were longer than those obtained with high-density samples. This increase in insulation time with decreasing density, which apparently results from a lower thermal diffusivity, agrees with the experimental trend reported in reference 1.

Material composition: The materials were also tested to determine the effect of their composition on insulation time. In view of the effect of material density discussed in the previous section, a low-density cork composite was tested extensively in both nitrogen and air. The data plotted in figure 8(b) show that the over-all performance of the cork is better than that of the plastic; however, the performance is affected more by air exposure at the higher heating rates. The difference in nitrogen and air at low heating rates does not agree with the measurements of Tellep, et al., presented in reference 19. However, the facility of reference 19 was a graphite heater through which nitrogen was passed and heated, and then oxygen added to the test stream. As indicated by Georgiev and Rose in reference 18, if the free oxygen content of the stream is depleted by combining with the hot graphite particles, the stream is, in effect, inert. This is a possible explanation for the difference between the present data and that of reference 19.

Test results presented in figure 9 show that, in general, the performance decreased as the density was increased. For example, cork, the lightest material having a density of 29 lb/ft^3 was the most effective in limiting the inward diffusion of heat, while the heaviest material, 50 N 50 P, which weighed 75 lb/ft^3 was the least effective. The quantitative dependence of insulation time upon density is readily seen in figure 9, where the ratio

$$\left(\frac{t_{\Delta T=300}}{W}\right) \Big/ \left(\frac{t_{\Delta T=300}}{W}\right)_{cork}$$

has been plotted as a function of initial material density for heating rates of 10 and 100 Btu/ft^2sec in a nitrogen stream. It will be noted that this ratio appears to be independent of heating rate, but the ratio will depend upon the gas composition since the cork data, as shown in figure 8(b), is a function of gas composition at both high and low heating rates. Unfortunately, the majority of the other materials had been tested solely in nitrogen so that insufficient data existed for a figure similar to figure 9 for air exposure.

Measurements of Insulation Efficiency

To compare the present results with those of other investigations, the data of figure 8 are combined to yield the insulation efficiency

$$\frac{Q}{W} = \frac{q(t_{\Delta T=300})}{W}$$

which is plotted as a function of q in figures 10(a) and (b). Note that for thin sections of material as the heating rate decreases, the insulation efficiency also decreases in spite of an increase in the insulation time. This apparent anomaly is due to the appearance of q in the numerator of Q/W, and to the percentage decrease in q far exceeding the percent increase in insulation time. For example, when q is decreased by a factor of 10 from 100 to 10 Btu/ft^2sec, the insulation time is increased by a factor of 2.8. The variation of Q/W with q for a thicker sample (0.48 in.) of more dense (75 lb/ft^3) material (50 percent nylon, 50 percent phenolic nylon, ref. 1) is also shown in figure 9. It is noted immediately that when these data are extrapolated to the lower heating rates, the values of insulation efficiency are twice as large as those of the present test data. This apparent increase in performance could be due to either the thicker copper substrate (0.12 in.) or thicker material sample used in the tests of reference 1.

The effect of these two model parameters on the insulation efficiency was obtained both analytically and experimentally. The previously mentioned computer program had provisions for adding substructure material to the composite ablation material. Therefore, the variation of Q/W with q was computed for various thicknesses of substructure, for a material thickness of 0.1 inch. The

calculations show that at high heating rates, the substructure thickness had little effect, since the ratio of heat stored in the calorimeter to that transmitted to the surface was small. However, at low heating rates, the heat stored in the substrate becomes an appreciable fraction of the incident flux. Hence, as the heat capacity is increased (i.e., substrate becomes thicker) the insulation efficiency apparently increases. Measurements of the back-face temperature rise were also made with test samples having no substrate (i.e., thermocouples attached directly to the material), and these measurements agreed with the calculated trend; that is, at high heating rates, there was no difference in $t_{\Delta T=300}$, while at low heating rates $t_{\Delta T=300}$ was decreased from the values obtained from models having substrates. The reduction was only 10 percent and thus it may be concluded that the heat-sink effect of thick substrates is only of consequence when the heating rate is low.

In order to investigate the effect of test sample thickness on Q/W, let us approximate the form of the temperature-time histories shown in figure 5, by the straight line as shown in sketch (a),

$$t = t_i + \frac{\partial t}{\partial T}(T - T_i) \qquad (1)$$

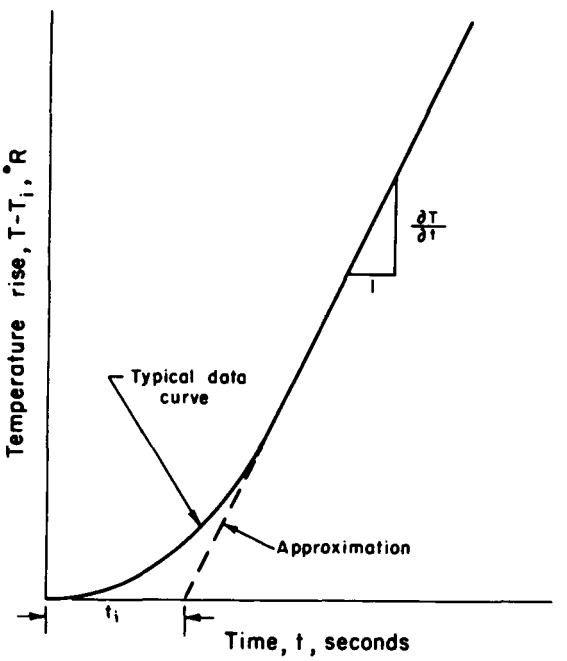

Sketch (a)

where t_i is the transient time for the heat pulse to penetrate to the back surface and $\frac{\partial t}{\partial T}$ is proportional to the heating rate to the back surface (the difference between the net heating rate to the surface and the rate of heat storage in the material). Combining this equation with the expression for Q/W, we obtain

$$\frac{Q}{W} = \frac{[t_i + (\partial t/\partial T)\ 300]q}{\rho_i L_i} \qquad (2)$$

where t_i and $\partial t/\partial T$ are both functions of L_i and q,

$$t_i = f_1(L_i, q)$$

$$\frac{\partial t}{\partial T} = f_2(L_i, q)$$

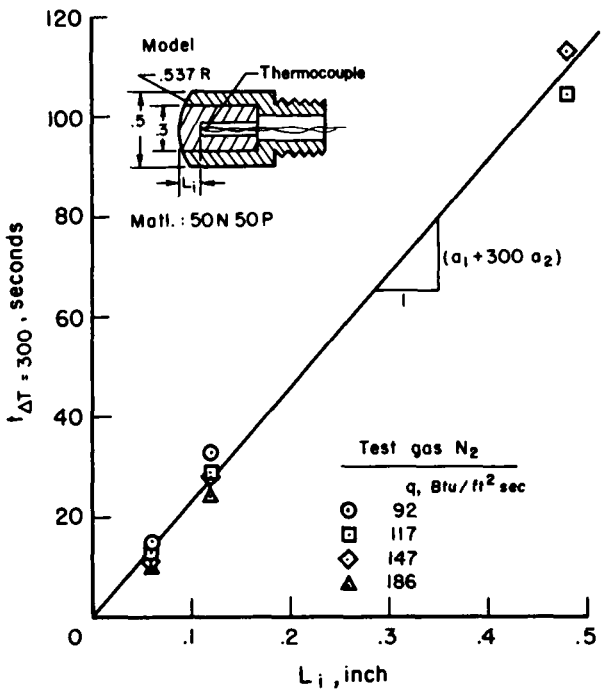

Sketch (b)

To obtain the functions f_1 and f_2, test samples similar to those used in reference 5 (see also sketch (b)) were constructed of the material 50 N 50 P to represent sample thicknesses of 0.060, 0.120, and 0.50 inch. The models were used to minimize the radial conduction of heat from the sides of the model which becomes appreciable for a 0.5 inch body diameter when the test sample length exceeds 0.20 inch. The samples were tested at heating rates of 92, 117, 147, and 186 Btu/ft^{2}sec. The results indicated that both t_i and $\partial t/\partial T$ increased linearly with increasing length and were relatively insensitive to q in the range $(92 < q < 186)$. Therefore,

$$t_i \cong a_1 L_i \text{ and } \frac{\partial t}{\partial T} \cong a_2 L_i \qquad (3)$$

which substituted in equation (1) yields

$$t_{\Delta T=300} \cong (a_1 + 300a_2)L_i \qquad (4)$$

A comparison of this equation with the data is shown in sketch (b). It must be remembered that the derived equation is approximate, and may not be applicable when the heating rate differs appreciably from the range of the measurements. Combining equations (4) and (2) yields

$$\frac{Q}{W} \cong \frac{(a_1 + 300a_2)L_i q}{L_i \rho_i} \cong \frac{a_3 q}{\rho_i} \qquad (5)$$

Equation (5) shows that Q/W is independent of L_i at heating rates from 92 to 186 Btu/ft^{2}sec which agrees with the data of figure 10(a). However, at the lower heating rates, if it is assumed that ablation and charring are confined to a narrow region near the surface, the conduction process may be represented as a conventional one-dimensional slab problem. The Fourier modulus $\alpha t/L_i^2$ now determines both t_i and $\partial t/\partial T$, and the simple empirical relationships of equation (3) are no longer valid. Thus, the low heating rate values of Q/W are dependent on the sample thickness, with higher values being obtained as the thickness is increased. One must, therefore, be careful in using this parameter to "generalize" arc-jet wind-tunnel data. In fact, it may be necessary to duplicate the heat shield thickness, bonding agent, and substructure as well as the shape and duration of the heat pulse if design data are required.

Ablation Rate

The choice of a thermal protection material depends on more parameters than insulation efficiency alone. This is only a figure of relative merit and, as such, can be used to compare materials in a given environment. One of the most important of these parameters in controlling the over-all system weight is the ability of the material to resist surface erosion. That is, the total ablation rate, which includes material removed by oxidation as well as thermal and mechanical forces, must also be considered when designing a full-scale heat shield. It must be noted that even though cork is a more efficient insulator than the lightweight phenolic, almost all the original material was consumed by ablation during its exposure to the stream. However, the lightweight phenolic although charred receded only a small amount. Thus, the plastic material could furnish some thermal insulation on the second pass of a skip-type trajectory and on a full-scale vehicle would limit dimension changes which might alter its aerodynamic characteristics.

CONCLUDING REMARKS

The insulation behavior of several charring materials was evaluated experimentally in both arc-heated nitrogen and air at low and high heating rates. The materials behaved more favorably when exposed to high heating rates for short times as opposed to a long time low heating rate exposure. A degradation of performance, which is attributed to combustion, was observed when the test gas was air. The most pronounced reduction occurred at the lower heating rates where it appears the combustion and convective heat inputs are comparable in magnitude. All the materials exhibited this same trend with regard to the effect of heating rate and test stream composition; however, the performance level was different for each material. In general, the lower density materials, such as cork, were the most efficient over the entire range of test conditions.

The present study was confined to the behavior of materials under laminar, attached flow conditions and it is recognized that on the afterbody of a full-scale reentry vehicle where the heating rate is low, there may be regions which experience turbulent, separated flow. Therefore it would be worthwhile to investigate the effects of these conditions on the performance of charring materials.

Ames Research Center
National Aeronautics and Space Administration
Moffett Field, Calif., March 29, 1963

REFERENCES

1. Brooks, William A., Jr., Swann, Robert T., and Wadlin, Kenneth L.: Thermal Protection for Spacecraft Entering at Escape Velocity. Society of Automotive Engineers, presented at National Aeronautics Meeting, April 3-6, 1962.

2. Schmidt, Donald L., and Schwartz, Herbert S.: Experimental Evaluation Methods for Ablative Plastics. ASD-TR-61-691, Aeronautical Systems Division, Wright-Patterson Air Force Base, Ohio, March 1962.

3. Steg, L., and Lew, H.: Hypersonic Ablation. General Electric Rep. R62SD55, Presented at AGARD Hypersonic Conference TCEA, Belgium, April 3-6, 1962.

4. Staff, Chance Vought, Astronautics Division: Carbonized Plastic Composites for Hyperthermal Environments. ASD-TDR-62-352, Aeronautical Systems Division, Wright-Patterson Air Force Base, Ohio, June 1962.

5. Vojvodich, Nick S.: The Performance of Ablative Materials in a High Energy, Partially Dissociated, Frozen Nitrogen Stream. NASA TN D-1205, 1962.

6. Winkler, Ernest L., and Griffin, Roy N., Jr.: Effects of Surface Recombination on Heat Transfer to Bodies in a High Enthalpy Stream of Partially Dissociated Nitrogen. NASA TN D-1146, 1961.

7. Winkler, Ernest L., and Griffin, Roy N., Jr.: Measurements in a Frozen, Partially Dissociated, High-Speed Gas Stream. Proc. Second Symposium on Hypervelocity Techniques, Univ. of Denver, Denver Res. Inst. Plenum Press, N. Y., 1962., pp. 511-522.

8. Compton, Dale L., Winovich, Warren, and Wakefield, Roy M.: Measurements of the Effective Heats of Ablation of Teflon and Polyethylene at Convective Heating Rates From 25 to 420 Btu/ft^{2}sec. NASA TN D-1332, 1962.

9. Lees, Lester: Laminar Heat Transfer Over Blunt-Nosed Bodies at Hypersonic Flight Speeds. Jet Propulsion, vol. 26, no. 4, April 1956, pp. 259-69, 274.

10. Larson, Howard K.: Heat Transfer in Separated Flows. Jour Aero/Space Sci., vol. 26, no. 11, Nov. 1959, pp. 731-738.

11. Goldsmith, Alexander, Waterman, Thomas E., and Hirschhorn, Harry J.: Handbook of Thermophysical Properties of Solid Materials. Rev. ed., Macmillan Co., N. Y., 1961.

12. McAdams, William H.: Heat Transmission. Third ed., McGraw-Hill Book Co., N. Y., 1954.

13. Reynolds, M. M., Corruccini, R. J., Fulk, M. M., and Burley, R. M.: Radiometry. American Institute of Physics Handbook, Sect. 6g, McGraw-Hill Book Co., N. Y., 1957, pp. 64-82.

14. Selbo, M. L., and Lulling, R. M.: Effect of Rate of Temperature Rise on Adhesive Bonds in Steel. ASD-TDR-62-573, Wright-Patterson Air Force Base, Ohio.

15. Munson, T. R., and Spindler, R. J.: Transient Thermal Behaviour of Decomposing Materials, Part I. General Theory and Application to Convective Heating. IAS Paper 62-30, Jan. 1962.

16. Moore, Jeffrey A., and Zlotnick, Martin: Combustion of Carbon in an Air Stream. ARS Jour., vol. 31, no. 10, Oct. 1961, pp. 1388-1397.

17. Hartnett, J. P., and Eckert, E. R. G.: Mass Transfer Cooling With Combustion in a Laminar Boundary Layer. Heat Transfer and Fluid Mechanics Institute, June 19-21, 1958.

18. Georgiev, S., and Rose, P. H.: Effects of Carbon Contamination of Air on Ablation Arc Wind Tunnel Test Results. Rep. 113, AVCO-Everett Res. Lab., Dec. 1959.

19. Tellep, D. M., Levy, A. M., Sheppard, T. D., and Irwin, M.: Thermodynamic Evaluation of Materials Under Ascent Phase Heating Conditions. Preprint LMSC-895196. Spacecraft Thermodynamics Symposium, March 28, 1962.

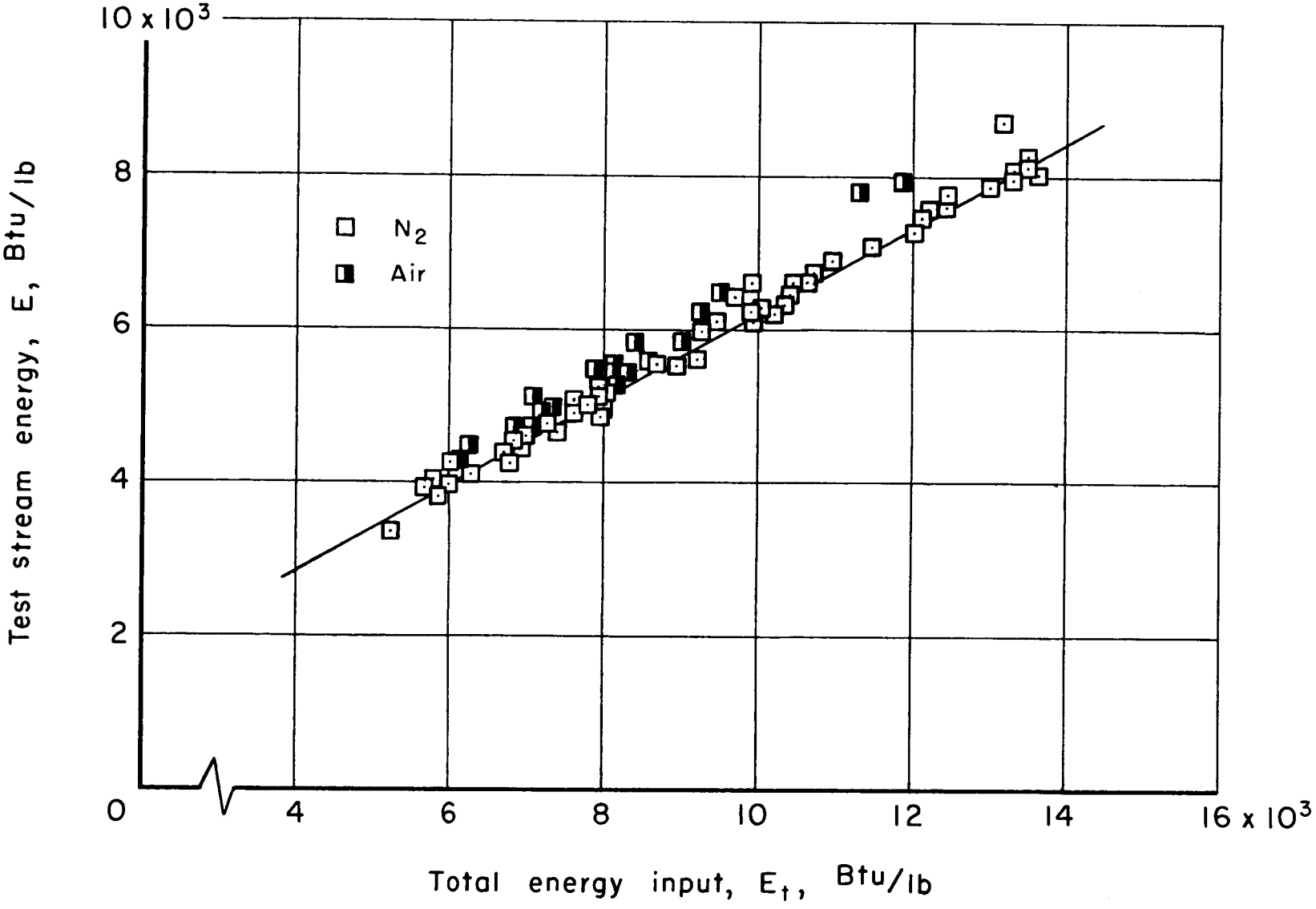

Figure 1.- Variation of test stream energy with total energy input.

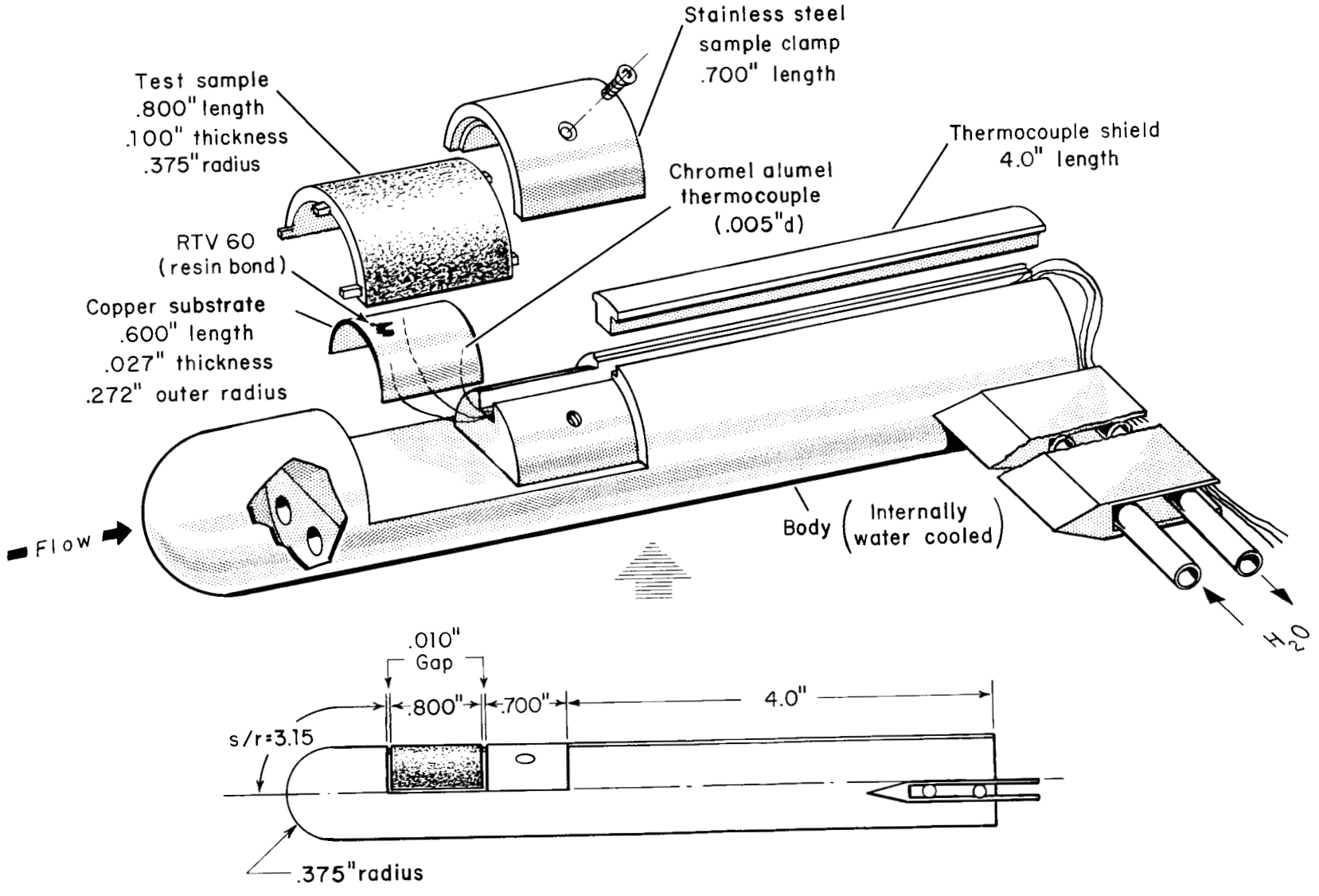

(a) Model 1 (half-cylinder; low heating rate).

Figure 2.- Insulation models.

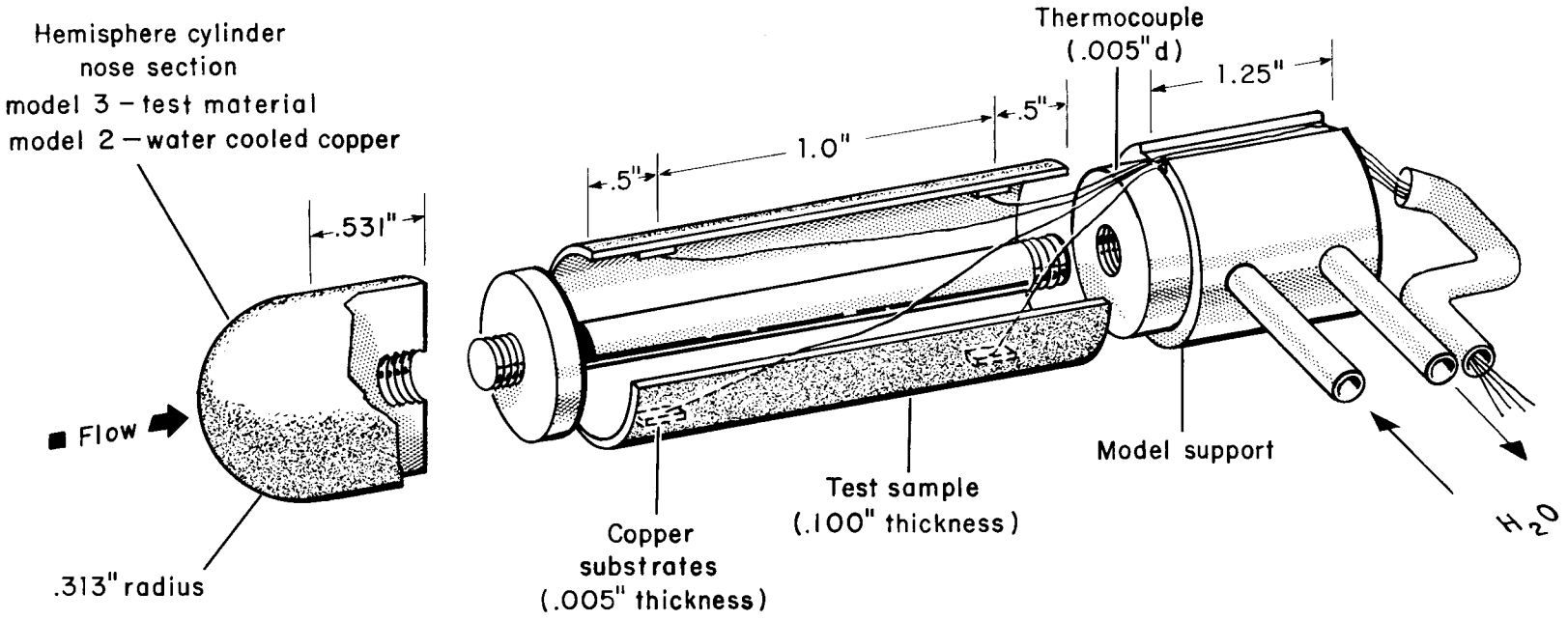

(b) Models 2 and 3 (full-cylinder, low heating rate).

Figure 2.- Continued.

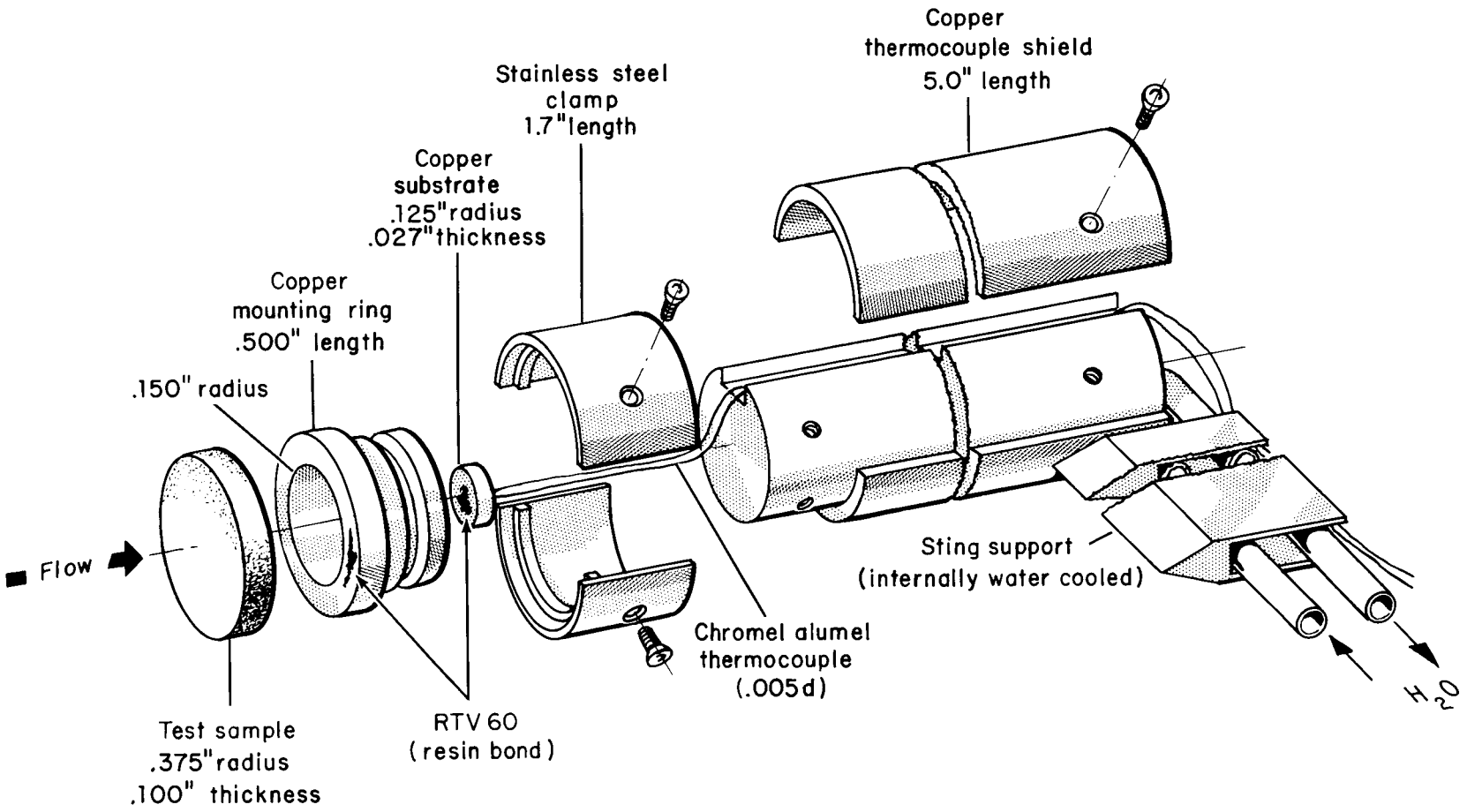

(c) Model 4 (stagnation point; high heating rate).

Figure 2.- Concluded.

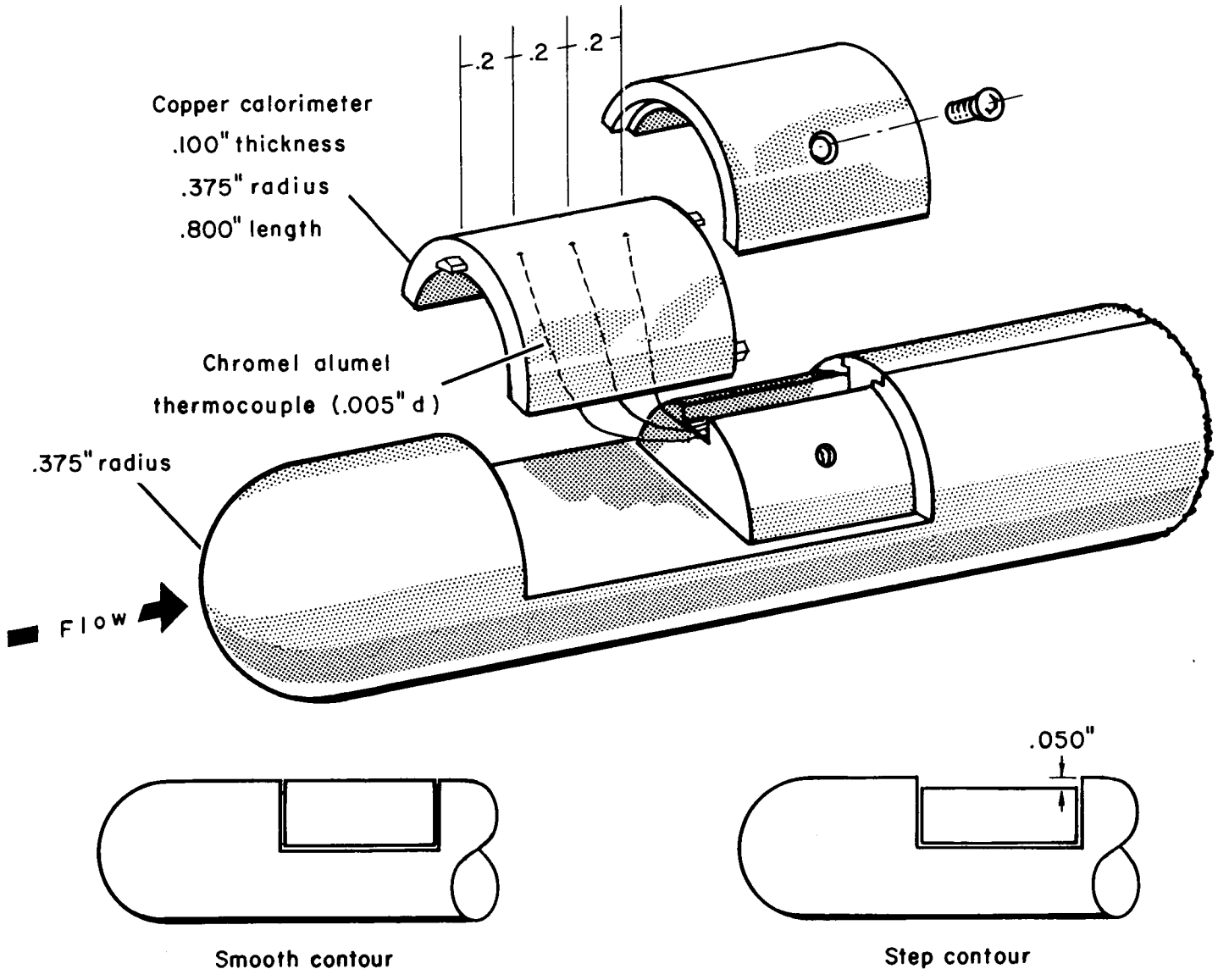

(a) Afterbody calorimeter models.

Figure 3.- Heat-transfer models.

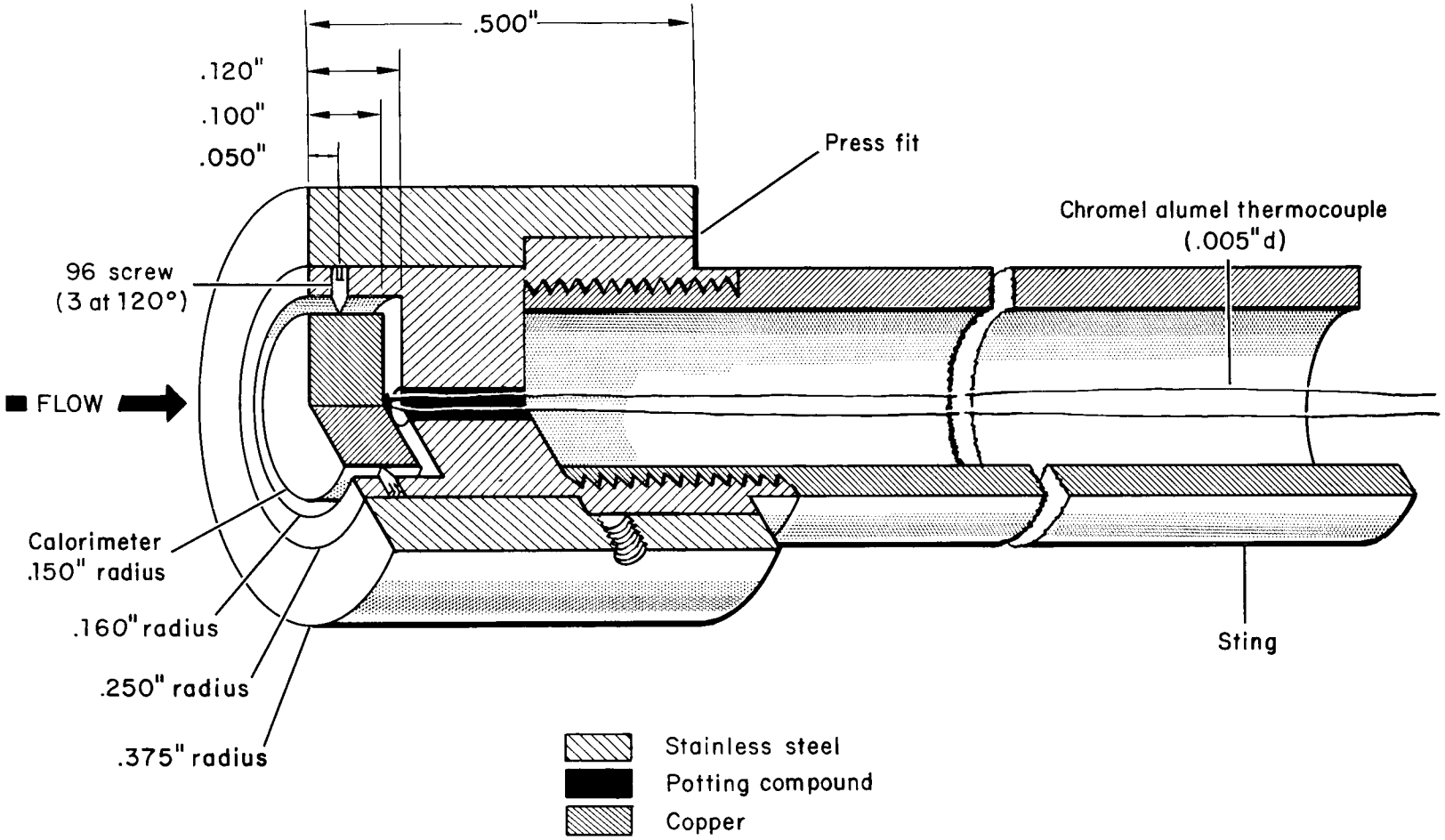

(b) Stagnation-region model.

Figure 3.- Concluded.

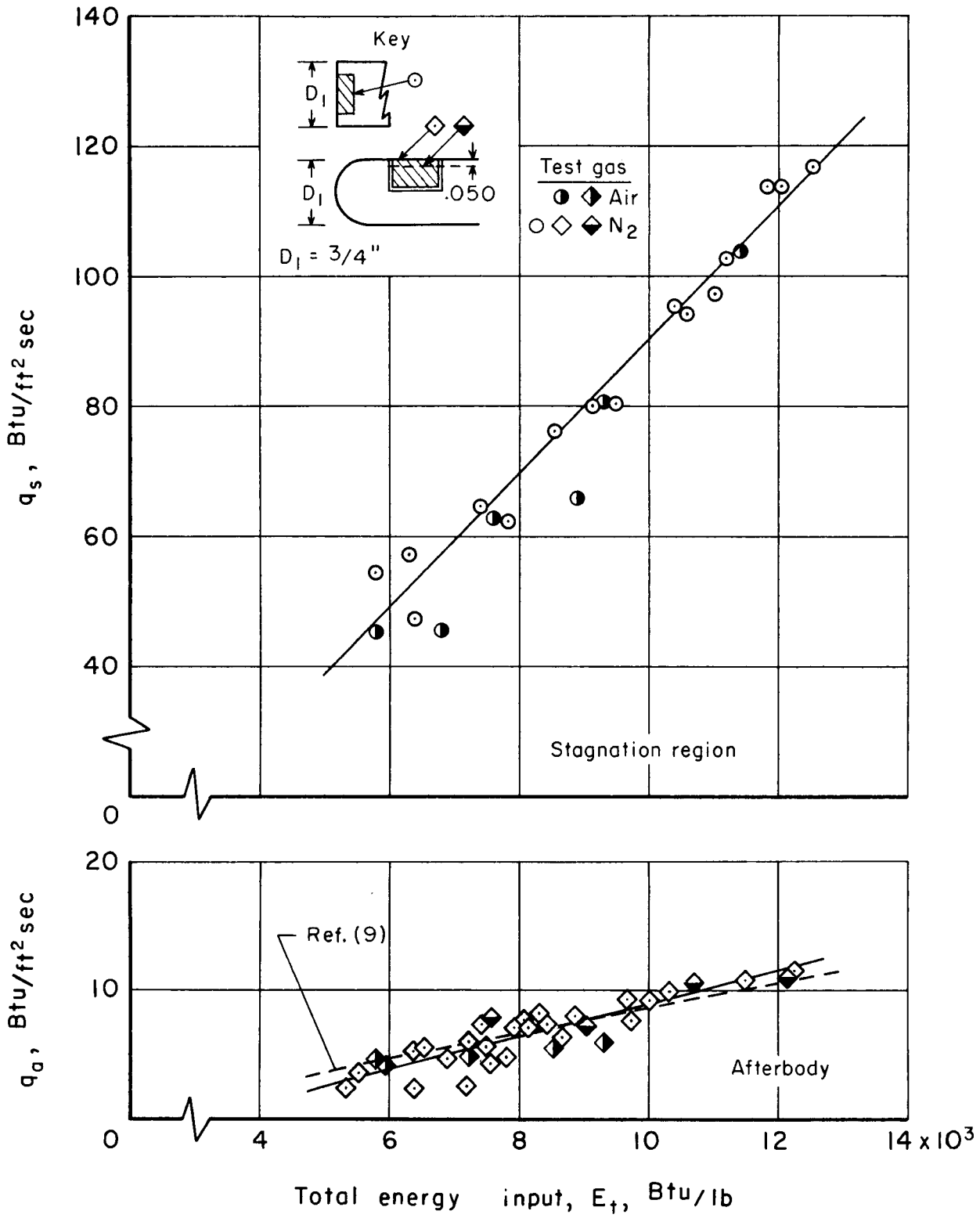

Figure 4.- Variation of afterbody and stagnation-region heat-transfer rate with total energy input.

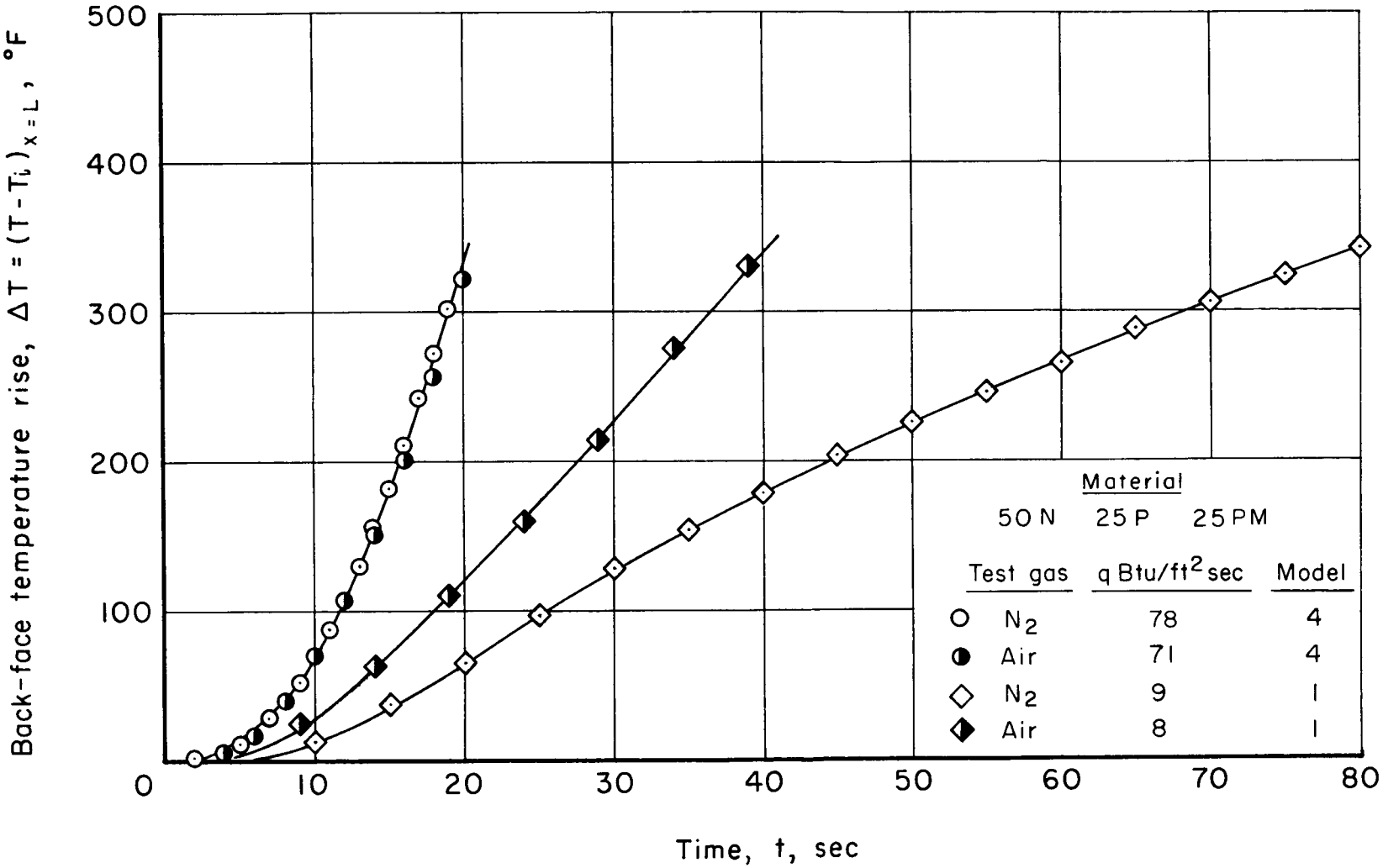

Figure 5.- Representative back-face temperature variations with time.

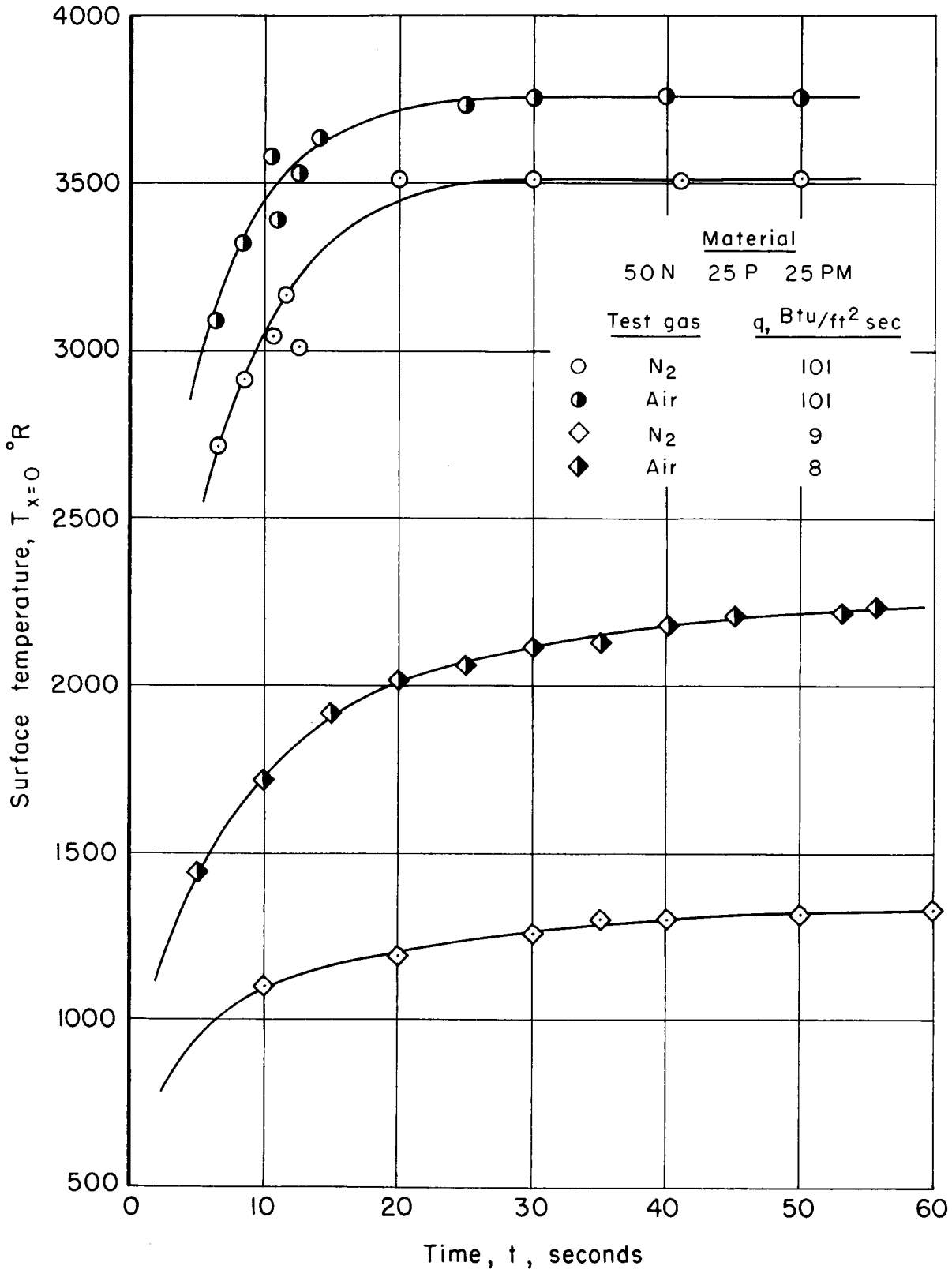

Figure 6.- Representative surface temperature variations with time.

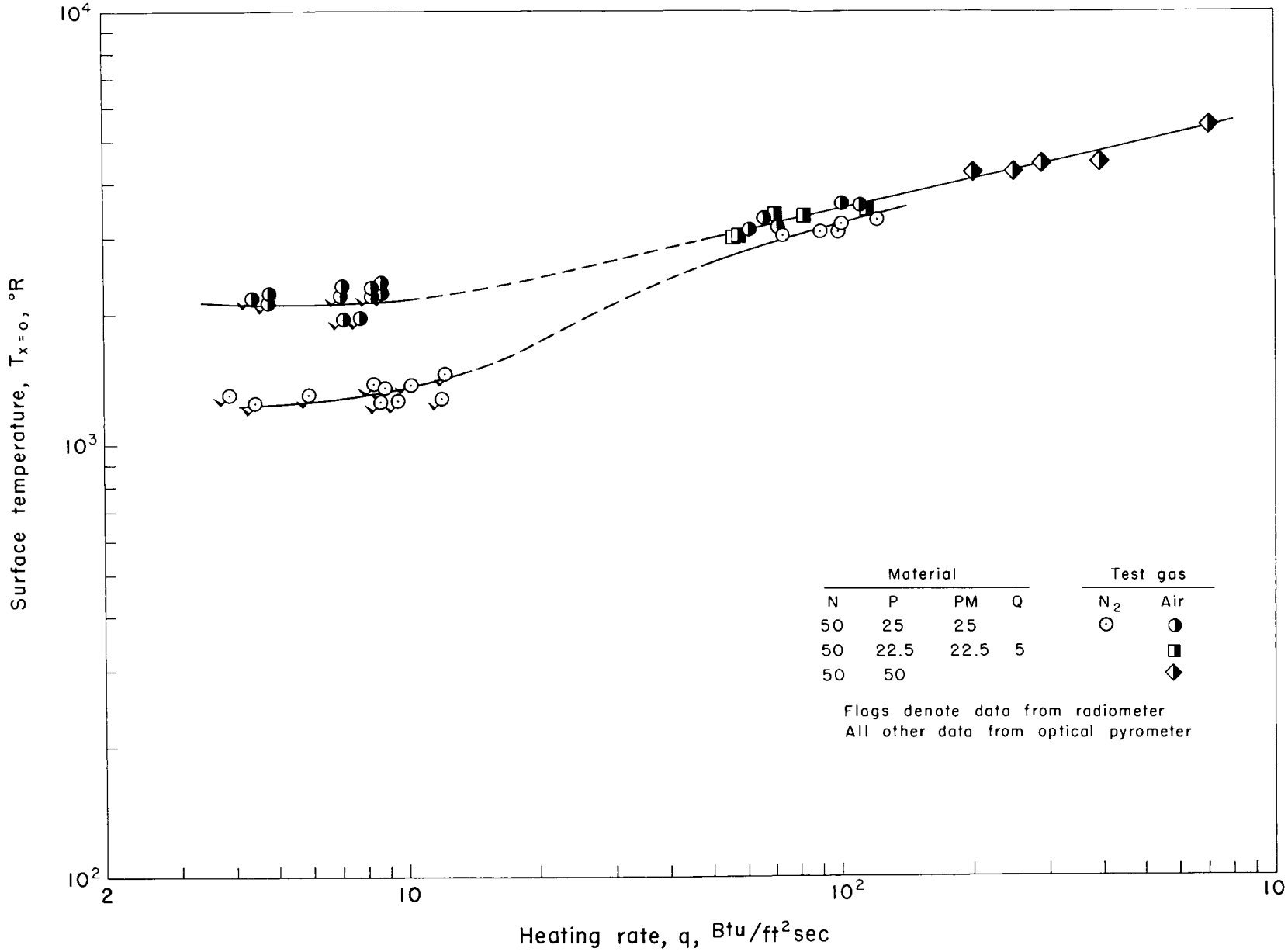

Figure 7.- Effect of heating rate and gas composition on steady-state surface temperatures.

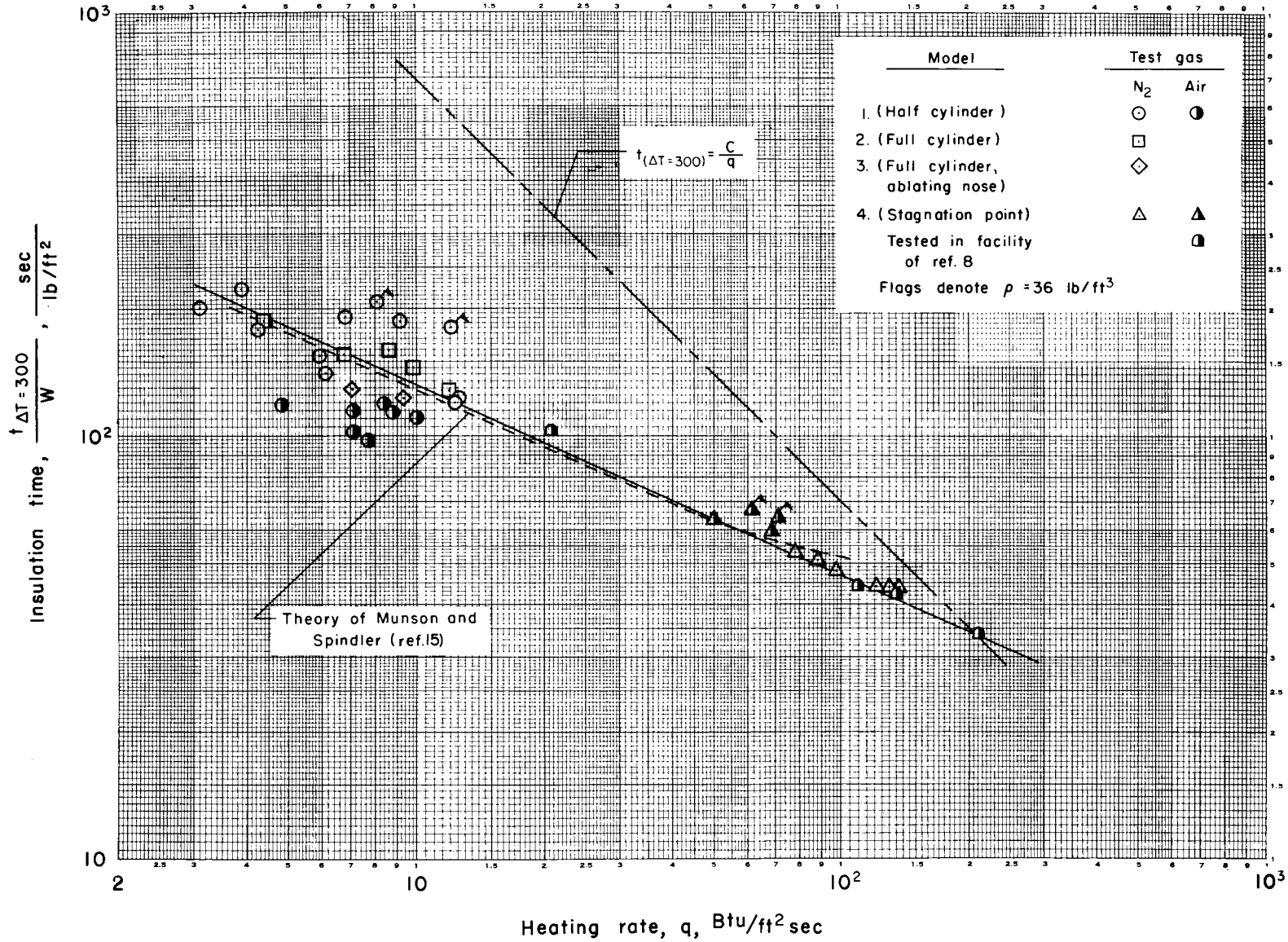

(a) Typical composite plastic, 50N 25P 25PM; ρ = 45 lb/ft^3 except as noted.

Figure 8.- Variation of insulation time with heating rate.

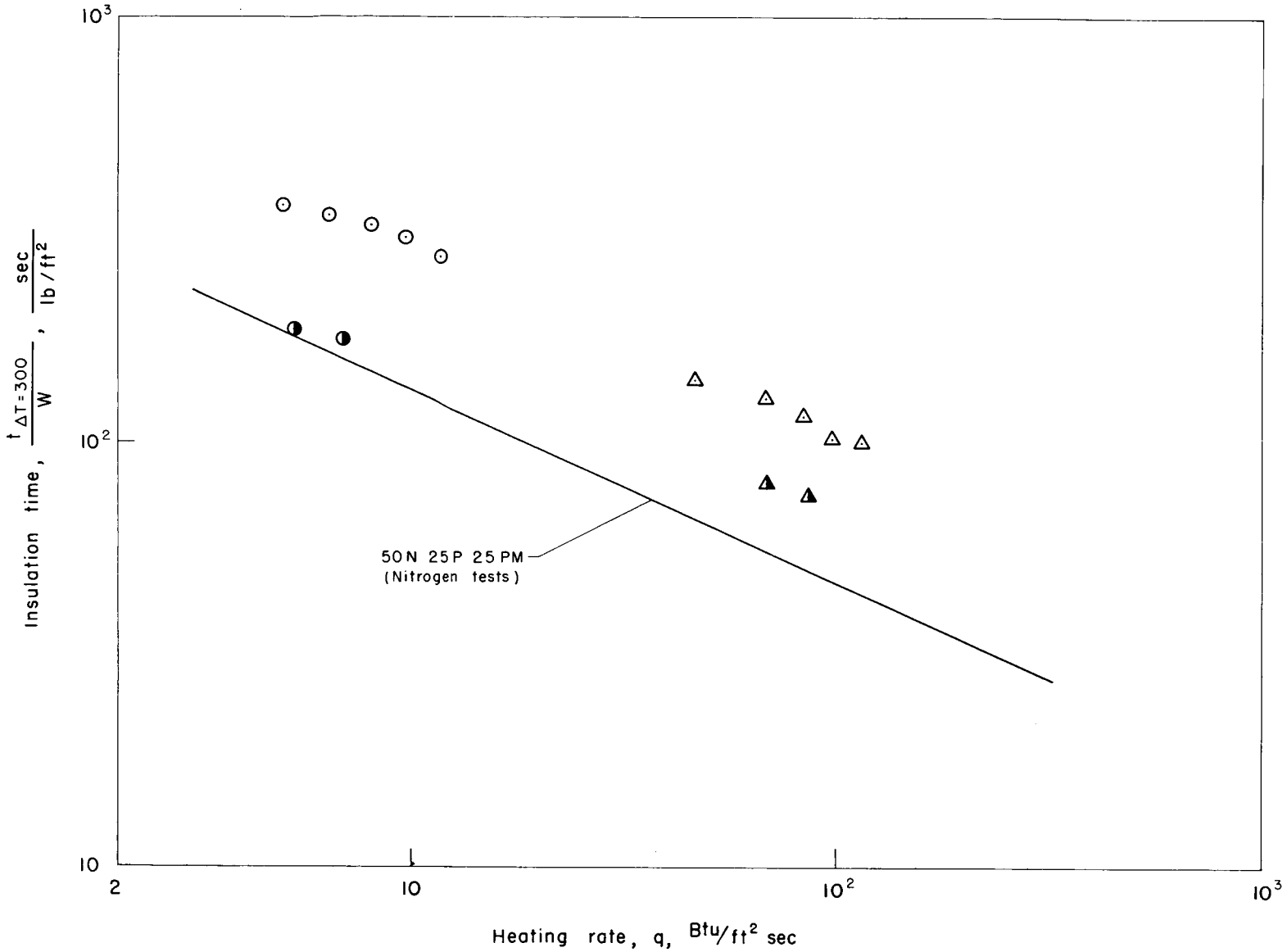

(b) Cork composition; ρ = 29 lb/ft^3.

Figure 8.- Concluded.

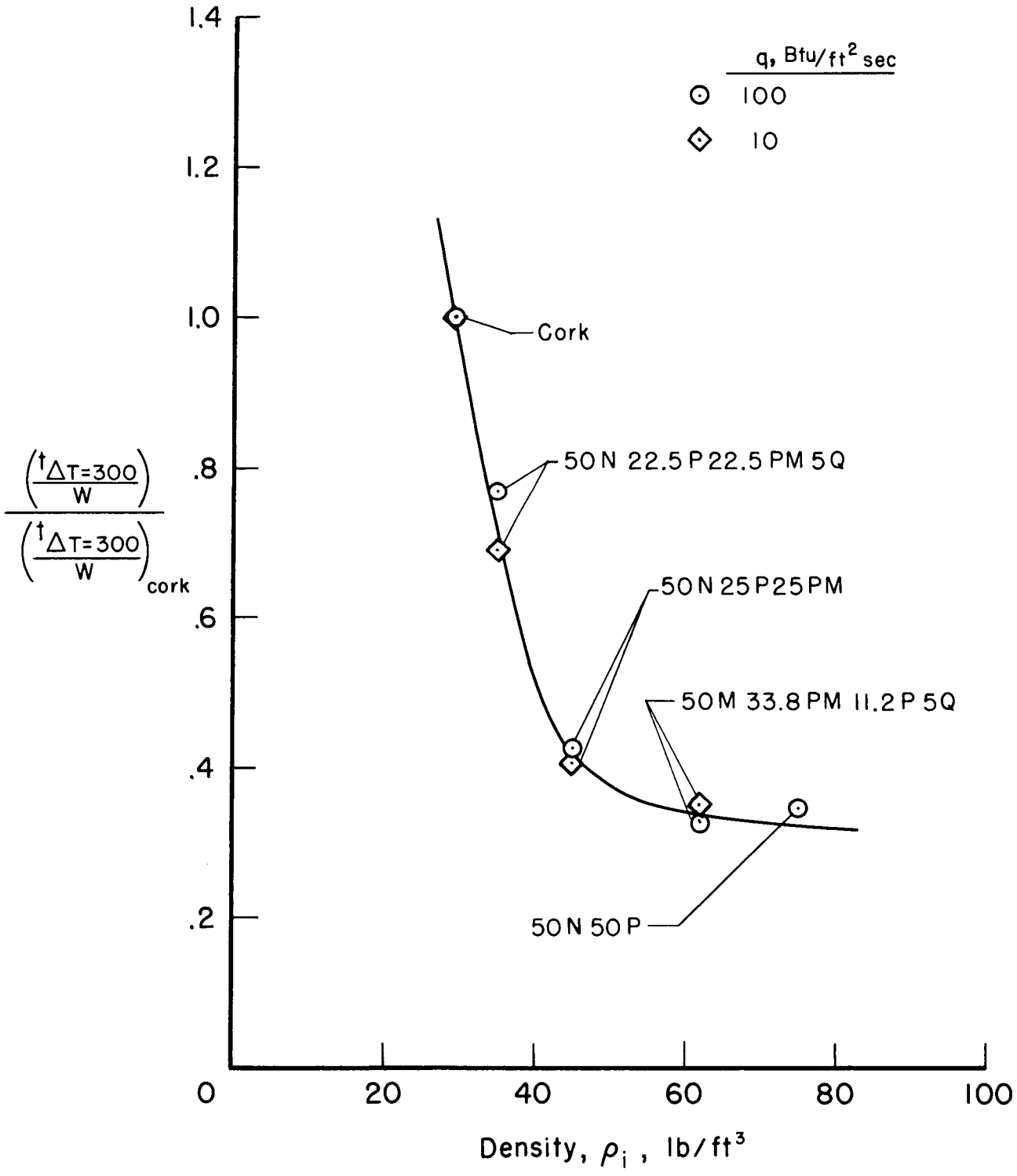

Figure 9.- Effect of initial material density on normalized insulation time for nitrogen tests; L_i = 0.1 inch.

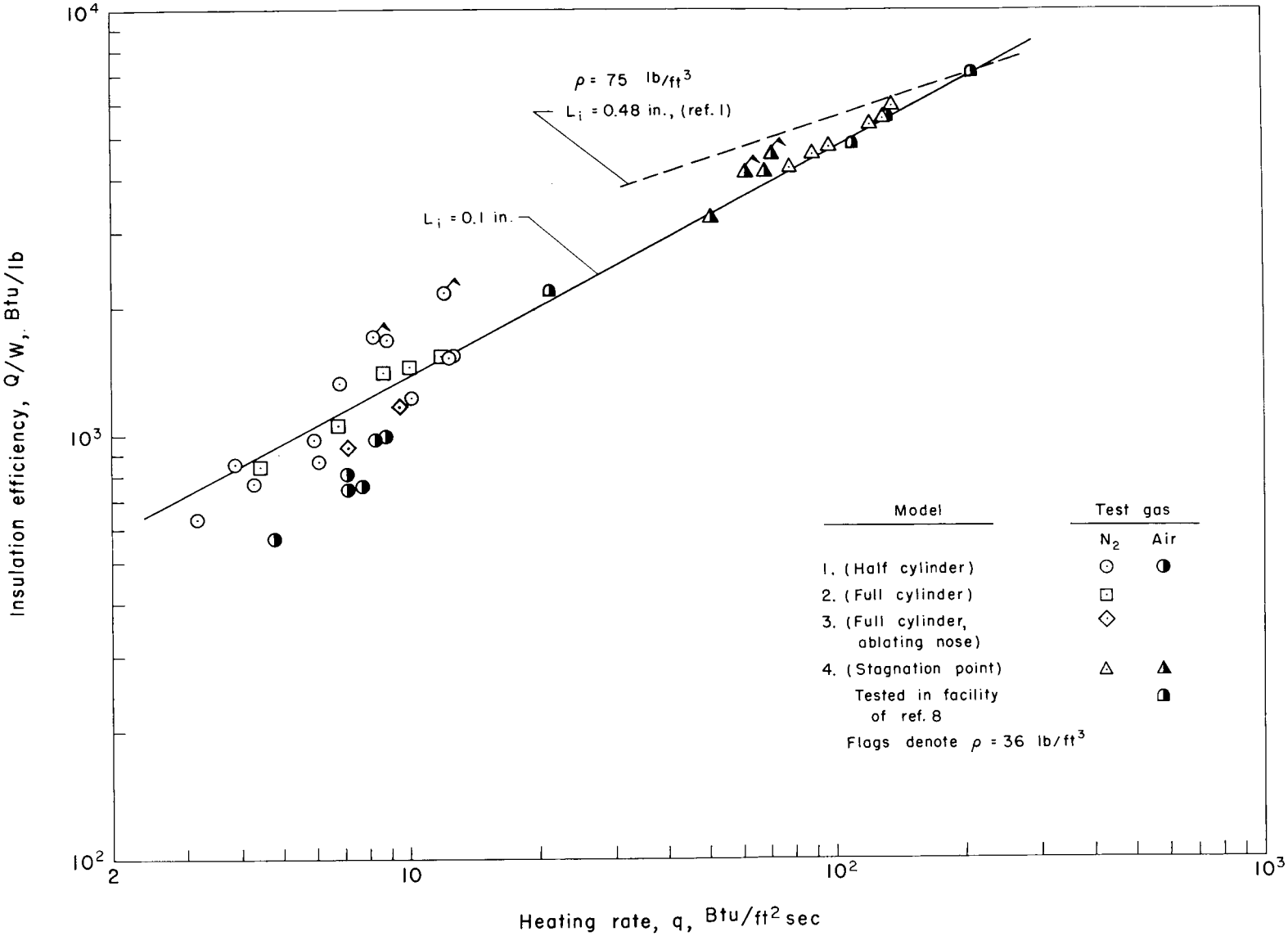

(a) Typical composite plastic, 50N 25P 25PM; ρ = 45 lb/ft^3 except as noted.

Figure 10.- Variation of insulation efficiency with heating rate.

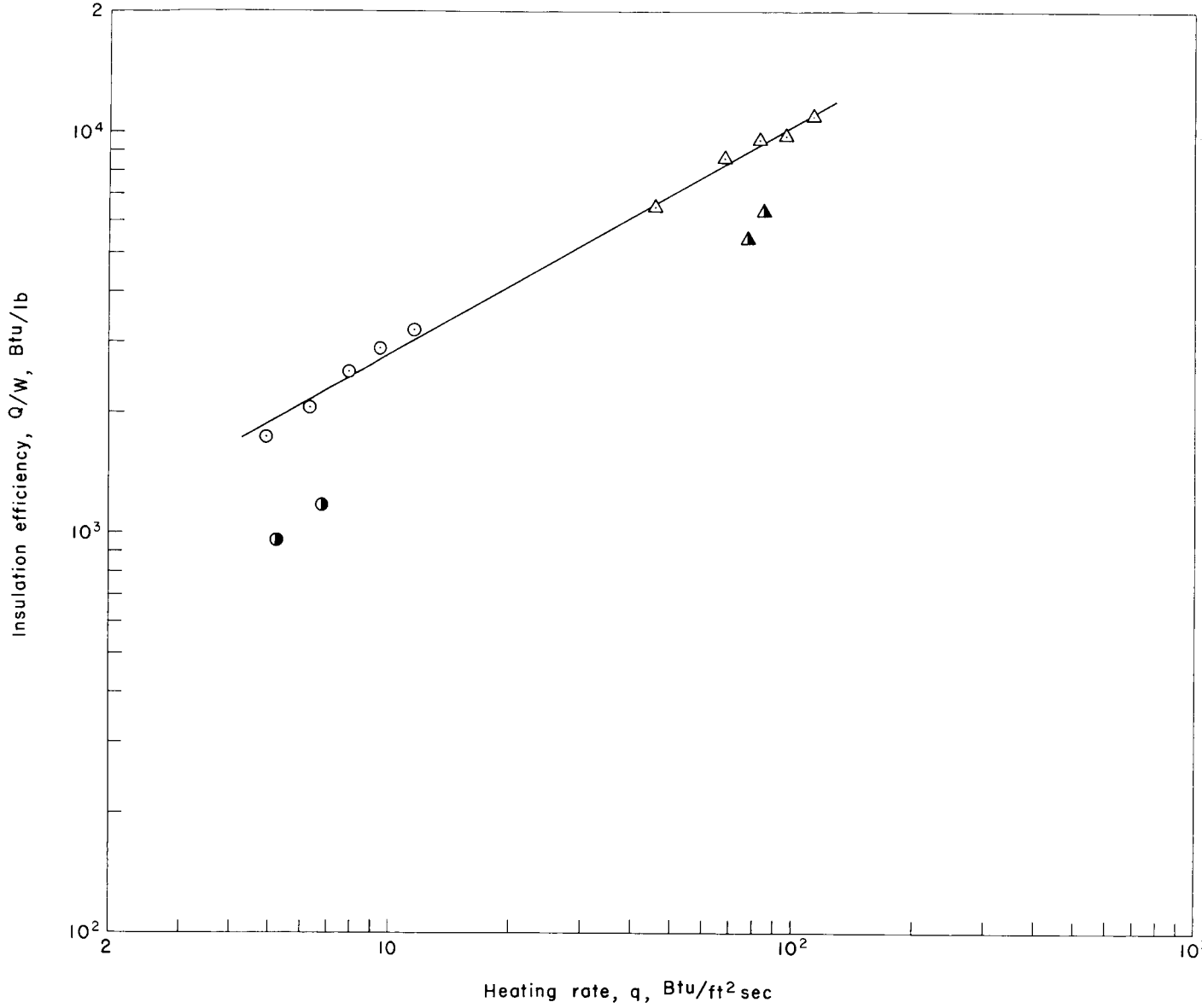

(b) Cork composition; ρ = 29 lb/ft^3.

Figure 10.- Concluded.